







Article

Organic Salt Hydrate as a Novel Paradigm for Thermal Energy Storage

Emanuela Mastronardo ^{1,*}, Emanuele La Mazza ², Davide Palamara ¹, Elpida Piperopoulos ^{1,2,3,*}, Daniela Iannazzo ¹, Edoardo Proverbio ¹ and Candida Milone ^{1,3}

- ¹ Engineering Department, University of Messina, Contrada di Dio, 98166 Messina, Italy; dpalamara@unime.it (D.P.); diannazzo@unime.it (D.I.); eproverbio@unime.it (E.P.); cmilone@unime.it (C.M.)
² CNR ITAE “Nicola Giordano”, Via Salita S. Lucia Sopra Contesse 5, 98126 Messina, Italy; emanuele.lamazza@itae.cnr.it
³ National Interuniversity Consortium of Materials Science and Technology (INSTM), 50121 Florence, Italy
* Correspondence: emastronardo@unime.it (E.M.); epiperopoulos@unime.it (E.P.)

Abstract: The use of inorganic salt hydrates for thermochemical energy storage (TCS) applications is widely investigated. One of the drawbacks that researchers face when studying this class of materials is their tendency to undergo deliquescence phenomena. We here proposed and investigated, for the first time, the possibility of using organic salt hydrates as a paradigm for novel TCS materials with low water solubility, that is, more resistance to deliquescence, a tendency to coordinate a high number of water molecules and stability under operating conditions. The organic model compound chosen in this study was calcium; 7-[[2-(2-amino-1,3-thiazol-4-yl)-2-methoxyiminoacetyl]amino]-3-[(2-methyl-5,6-dioxo-1H-1,2,4-triazin-3-yl)sulfanylmethyl]-8-oxo-5-thia-1-azabicyclo[4.2.0]oct-2-ene-2-carboxylate, known as calcium ceftriaxone, hereafter named CaHS (calcium hydrated salt), a water-insoluble organic salt, which can combine up to seven water molecules. The CaHS was prepared by precipitation from the water-soluble disodium triaxone. The thermal behavior of CaHS, in terms of stability and dehydration–hydration cyclability, was assessed. The material can operate in the temperature range of 30–150 °C, suitable for TCS. No deliquescence phenomena occurred upon exposure to a relative humidity (RH) between 10 and 100%. Its heat storage capacity, so far unknown, was measured to be ~595.2 kJ/kg (or ~278.6 kWh/m³). The observed heat storage capacity, thermal stability, and good reversibility after dehydration–hydration cycles highlight the potential of this class of materials, thus opening new research paths for the development and investigation of innovative organic salt hydrates.

Keywords: thermochemical energy storage; organic salt hydrate; deliquescence; thermogravimetric dynamic vapor sorption



Citation: Mastronardo, E.; La Mazza, E.; Palamara, D.; Piperopoulos, E.; Iannazzo, D.; Proverbio, E.; Milone, C. Organic Salt Hydrate as a Novel Paradigm for Thermal Energy Storage. *Energies* **2022**, *15*, 4339. <https://doi.org/10.3390/en15124339>

Academic Editor:
Massimiliano Renzi

Received: 17 May 2022

Accepted: 12 June 2022

Published: 14 June 2022

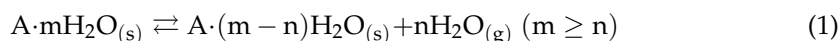
Publisher’s Note: MDPI stays neutral with regard to jurisdictional claims in published maps and institutional affiliations.



Copyright: © 2022 by the authors. Licensee MDPI, Basel, Switzerland. This article is an open access article distributed under the terms and conditions of the Creative Commons Attribution (CC BY) license (<https://creativecommons.org/licenses/by/4.0/>).

1. Introduction

Thermochemical energy storage (TCS) is a key technology that promotes more efficient use of energy from renewable sources [1–4] in the shift towards carbon-free renewable energy sources, which are inherently intermittent [5]. For example, while solar energy is the primary renewable energy source, its diurnal nature generates a mismatch between energy supply and demand. Therefore, developing an efficient TCS technology that allows storage of low-grade thermal energy and supplies it on demand can help guarantee energy security. Compared to sensible and latent heat storage [6], TCS offers higher energy density, heat supply available on request (namely, long-term heat storage), and lower heat losses [7]. Higher energy density makes thermochemical heat storage systems more compact, whereas lower heat losses and the dispatchability of the stored heat on demand make it more suitable for long-term energy storage. Currently, TCS technologies are based on inorganic salt hydrates, which involve a reversible solid–gas reaction [8–10]:



The reagent (the solid hydrated salt) is converted, through an endothermic process (charging step), to products that consist of a totally or partially dehydrated solid salt and gaseous water. To avoid recombination of the products, the water is removed and stored for re-use in the discharging step. The reverse rehydration reaction of the dehydrated salt with water vapor, being exothermic, releases heat on demand [11]. The rehydration reaction is fully reversible if the salt recovers the total number of crystal water molecules. However, in some cases, the hydration product is a saturated salt solution rather than a salt hydrate. This process is called deliquescence, i.e., a substance sorbs water vapor from the environment and gradually dissolves to form a solution at a critical relative humidity (RH) value, the deliquescence relative humidity (DRH) [12]. The deliquescence phenomenon implies some severe drawbacks, such as chemical instability. A liquid film forms on the surface of the salt crystal, thus inhibiting the rehydration reaction (e.g., in case of the LiCl, LiBr, CaCl₂) [10,13]; the sorbate mass transfer into the system is hindered, causing issues such as high-pressure drops and ultimately system failure, as well as corrosion issues due to the dripping of the salt solution onto other metal components of the system. In other cases, the deliquescence RH value limits the operating range, as in the case of MgSO₄, despite its very high potential heat storage capacity (2.3 GJ/m³).

The high potential of such systems [8] (with an average enthalpy of reaction of ~55.2 kJ per mole of water [14,15]) warrants further investigation to solve this issue. Salt hydrates can be embedded into porous matrices (such as carbon foams, expanded natural graphite, zeolite, vermiculite, silica gel, etc.) to prevent deliquescence and improve water transport into the materials [16–18]. Nevertheless, such strategies often fail to overcome these challenges without efficiency loss [3]. Microencapsulation is another approach for the stabilization of salt hydrates; salt particles are enveloped with a second inherently stable material to prevent coalescence or agglomeration. However, this methodology presents stability problems due to salt leakage, and the matrices themselves already strongly affect the equilibrium of the reaction shown in Equation (1), thus leading to an efficiency decrease [19,20]. Indeed, it is essential that water vapor can escape through the encapsulation material.

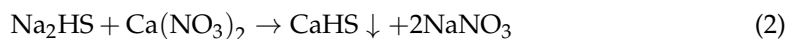
This work aims to explore new strategies for developing suitable materials based on highly insoluble organic hydrated salts in order to reduce and/or avoid deliquescence phenomena under operating conditions, ensure the ability to coordinate a high number of water molecules, and ensure stability under operation conditions. To test this idea, calcium;7-[[2-(2-amino-1,3-thiazol-4-yl)-2-methoxyiminoacetyl] amino]-3-[(2-methyl-5,6-dioxo-1H-1,2,4-triazin-3-yl)sulfanylmethyl]-8-oxo-5-thia-1-azabicyclo[4.2.0]oct-2-ene-2-carboxylate, known as calcium ceftriaxone, hereafter named CaHS (calcium hydrated salt), was chosen as a model compound. It is a highly insoluble salt (water solubility product constant is $1.62 \times 10^{-6} \text{ mol}^2/\text{L}^2$ [21]) that easily precipitates from the extremely soluble disodium ceftriaxone upon the addition of calcium ions. It should be mentioned that disodium ceftriaxone, despite containing 3.5 H₂O molecules within its crystal structure, cannot be taken under consideration as a TCM due to its high solubility [21]. It is reasonable to assume that in CaHS the hard acid Ca²⁺ can easily interact with the hard base H₂O and coordinate an expected range of 6–8 water molecules [22,23], according to the most stable coordination number of the calcium aquaone complex. We here carried out a study on the thermochemical behavior of CaHS for TES applications. Its heat storage capacity, not available in the literature, was estimated.

2. Materials and Methods

2.1. Synthesis of Calcium Ceftriaxone (CaHS)

CaHS was prepared using disodium ceftriaxone hemiheptahydrate (from now on referred to as Na₂HS, TOWA PHARMACEUTICAL CO., LTD., Osaka, Japan) as the precursor. Then, 15 mL of 0.08 M Na₂HS aqueous solution was added dropwise to 20 mL

of 0.166 M $\text{Ca}(\text{NO}_3)_2 \cdot 4\text{H}_2\text{O}$ (Sigma-Aldrich, St. Louis, Missouri, USA, $\geq 99.0\%$ purity) aqueous solution, inducing the formation of a pale yellow precipitate according to the following reaction:



Upon digestion for 3 h, the solid was separated by vacuum-assisted filtration and washed with H_2O to remove all the soluble unreacted reagents and with diethyl ether to remove the excess of physisorbed water. The product was dried at room temperature overnight under a relative humidity of $\sim 50\%$.

The yield of the exchange reaction of Na^+ with Ca^{2+} (Equation (2)) was evaluated by measuring the moles of Ca^{2+} present in the final product with respect to the theoretical amount, assuming that the Ca^{2+} to Na^+ replacement ratio is 1:2. The amount of calcium present in the solid was determined by a permanganometric redox titration on a weighted sample of CaHS (as reported in ESI Supplementary SI.1). The reaction yield, given by the ratio $100 \cdot n_{\text{experimental}}(\text{mol}) / n_{\text{theoretical}}(\text{mol})$, was determined to be $99.2 \pm 2\%$.

2.2. Chemical, Physical, Structural, Morphological, and Thermochemical Characterization of CaHS

Morphological studies were performed using scanning electron microscopy (SEM, FEI Quanta 450, Thermo Fisher Scientific, Waltham, Massachusetts, USA). Additionally, chemical analysis was performed along with the morphological studies using energy-dispersive X-ray spectroscopy (EDAX, Ametek, Tokyo, Japan) at an acceleration voltage of 20 kV. The crystal structure was analyzed via X-ray powder diffraction (XRD, D8 Advance Bruker diffractometer, Billerica, Massachusetts, USA, Bragg–Brentano theta-2theta configuration, $\text{Cu K}\alpha$, 40 V, 40 mA, $0.05^\circ/\text{s}$ scan rate). Fourier transform infrared spectroscopy (FTIR, Cary 600 Series FTIR Spectrometer, Agilent, Santa Clara, CA, USA) was performed in transmission mode in a wavenumber range from 400 cm^{-1} to 4000 cm^{-1} with a spectral resolution of 4 cm^{-1} and a scan number of 46 cm^{-1} .

To evaluate the thermal stability of the material, a sample aliquot ($\sim 10 \text{ mg}$) was heated (by $10^\circ\text{C}/\text{min}$) from r.T. up to 350°C in a vertical reactor under an inert gas flow (Ar $100 \text{ mL}/\text{min}$). The gaseous evolved species were analyzed through a mass spectrometer (MS, Discovery, TA Instruments, Waters Corporation, Milford, MA, USA) at the reactor outlet of the exhaust gases.

The material thermochemical behavior was evaluated via thermogravimetric analysis (TG, STA Jupiter F3 Netzsch, Selb, Germany). The analysis was carried out under an inert atmosphere ($120 \text{ mL}/\text{min N}_2$) using a holed Pt crucible and a sample mass of $\sim 10\text{--}20 \text{ mg}$. During the experiment, the sample was heated from r.T. up to 200°C by $10^\circ\text{C}/\text{min}$.

Differential scanning calorimetry (DSC, DSC8000 Perkin Elmer, Waltham, MA, USA) analyses were carried out to determine the dehydration reaction enthalpy. The instrument was calibrated with In and Zn elements, and it was equipped with a liquid nitrogen cooler to decrease the sample below r.T. and accurately control the heating and cooling rates. In a typical procedure, the sample ($\sim 8\text{--}10 \text{ mg}$), placed in disposable aluminum pans, was heated to the target temperature under an inert atmosphere ($20 \text{ mL}/\text{min N}_2$). A baseline was obtained by carrying out the same measurement without the sample (blank test) and subtracting the sample's test curve. An empty crucible was used as a reference and placed in the reference furnace. Two types of measurements were carried out: a ramp from 10 to 200°C (heating rate of $10^\circ\text{C}/\text{min}$) and an isothermal at 150°C for 2 h (heating rate of $30^\circ\text{C}/\text{min}$).

The relative density of the powder was measured using a helium pycnometer (Accupyc II 1345, Micromeritics, Norcross, GA, USA).

2.3. Dehydration–Hydration Cycles

In order to perform the dehydration–hydration cycles in a controlled (temperature, RH) and measurable (mass change) environment, dehydration–hydration cycles of CaHS

were subsequently performed using a thermogravimetric dynamic vapor sorption system (DVS Vacuum Surface Measurement Systems). The system consisted of a micro-balance (precision of $\pm 0.1 \mu\text{g}$) and a water vapor pressure flow controller placed in the measuring chamber. Before the tests, the sample was dehydrated at $150 \text{ }^\circ\text{C}$ under vacuum for 2 h. Each dehydration–hydration cycle was performed in isothermal mode, at $30 \text{ }^\circ\text{C}$ (the lowest controllable and achievable temperature), and with varying the RH from 0 to 90%. At each RH set value, the material was allowed to equilibrate. ESI was available in Supplementary SI.2 for a complete description of the performed test.

The mass change ($\Delta m(\%)$) associated with the water uptake/release was calculated according to the following equation:

$$\Delta m(\%) = \frac{m(\text{RH}, T_s) - m_0}{m_0} \times 100 \quad (3)$$

where $m(\text{RH}, T_s)$ is the equilibrium weight of the sample at a specific water vapor pressure and sample temperature, and m_0 is the dehydrated sample weight.

In order to evaluate the moles of H_2O per mole of CaHS, the following equation was applied:

$$n_{\text{H}_2\text{O}} = \frac{M_{\text{hyd}} - M_{\text{anh}}}{M_{\text{H}_2\text{O}}} \quad (4)$$

where M_{anh} is the molar mass of the anhydrous CaHS (592.75 g/mol), and M_{hyd} is the molar mass of the hydrated salt calculated as:

$$M_{\text{hyd}} = M_{\text{anh}} \left(1 + \frac{\Delta m(\%)}{100} \right) \quad (5)$$

3. Results and Discussion

3.1. CaHS Chemical Analysis, Structural, and Morphological Characterization

For completeness, a comparison between CaHS and its precursor, Na_2HS (JCPDS # 71-1637), is given in terms of structure and morphology. As inferred from the XRD analysis reported in Figure 1, the two materials exhibit different patterns, namely a structural modification caused by substituting the sodium cation with a calcium one. No repository files (CIF—Crystallographic Information File) were available for CaHS in the International Center for Diffraction Data database. Nevertheless, the patterns match with other results in the literature [22,24]. For completeness, the peaks list and d-spacing of the two materials are reported as Supplementary Information (Tables S1 and S2). Furthermore, CaHS exhibits significantly poorer crystallinity than Na_2HS . This structural change is also accompanied by a morphological modification as confirmed by SEM analysis (compare Figure 2a,b with Figure 2c,d). Indeed, while Na_2HS is made of large edgy particles, CaHS shows uniformly aggregated particles with irregular shapes. EDX elemental analysis on CaHS (Figure 2e) reveals the presence of calcium, oxygen, and sulfur in addition to carbon and nitrogen. No sodium signal is detected, thus excluding the presence of unreacted disodium ceftriaxone.

The coordination mode of the ceftriaxone anion towards Ca^{2+} was determined by comparing the FTIR spectra of Na_2HS and CaHS (Figure 3). After the complexation of ceftriaxone to the Ca^{2+} ion, the frequencies of both of the stretching vibrations of the carbonyl groups of β -lactam ((C=O) β -lactam) and triazine ((C=O) triazine) are shifted towards higher values, thus implying the involvement of the oxygen atoms in the coordination towards the Ca^{2+} ion. A shift towards higher wavenumbers at 3480 cm^{-1} is also observable for the band at 3427 cm^{-1} assigned to the (N–H) stretching vibration of the NH_2 group, supporting the hypothesis that the nitrogen atom of the amino group coordinates with the metal ion. The carboxylate group (COO) peak is shifted towards lower wavenumbers (1582 cm^{-1}). In agreement with previous findings [20], these shifts imply that the oxygen in the carboxylate group (COO) and the the oxygen carbonyl group (C=O) of β -lactam and the nitrogen in the amine group and the oxo group of the triazine ring are involved in

the coordination. The band at 3270 cm^{-1} is assigned to the stretching vibration of (O–H) group-coordinated water molecules.

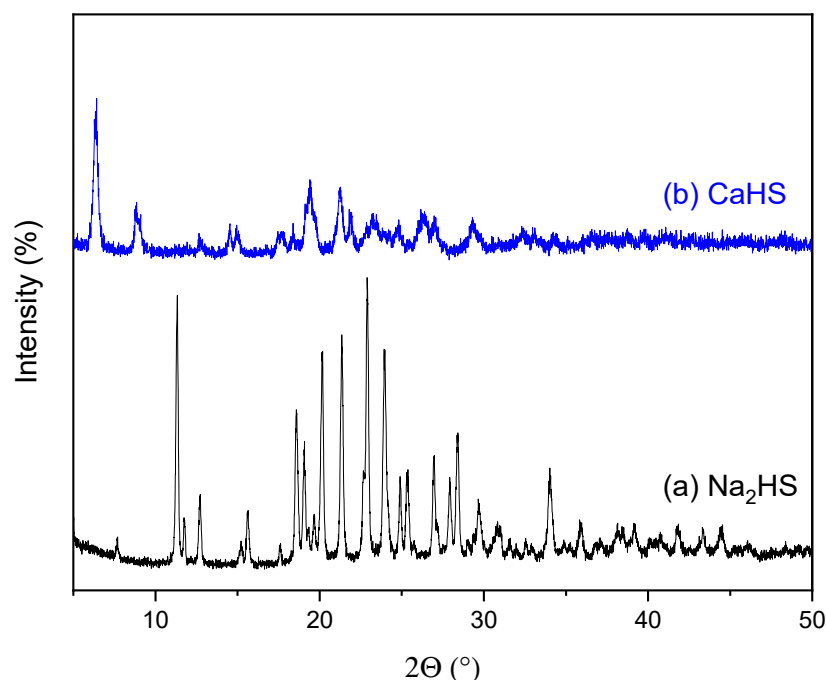


Figure 1. XRD spectra of (a) Na_2HS and (b) CaHS .

3.2. *CaHS Thermochemical Behavior and Thermal Stability*

The thermochemical behavior of the CaHS was evaluated via thermogravimetric analysis. The experiment carried out while ramping from r.T. to $200\text{ }^\circ\text{C}$ (Figure 4) found that the material undergoes continuous mass loss during the overall investigated temperature range (Figure 4). The measured mass loss was $\sim 13.1\%$, corresponding to the 4.3 water molecules initially contained in the as-synthesized material, assuming that the loss was entirely associated with the water release.

To verify if the mass loss up to $200\text{ }^\circ\text{C}$ was associated with water molecule dissociation and to determine the material thermal stability at higher temperatures, the following test was carried out: the material was heated from r.T. up to $350\text{ }^\circ\text{C}$ in a vertical reactor under inert atmosphere, and the gaseous evolved species was analyzed, using a mass spectrometer as a function of temperature, as shown in Figure 5. Two distinctive processes occurred in the investigated temperature range. The first, between 25 and $215\text{ }^\circ\text{C}$ and in agreement with TG data (Figure 4), consisted of the dehydration process, as confirmed by the detected mass spectrum corresponding to the molecular species with a molar mass of 18 g/mol . However, beyond $215\text{ }^\circ\text{C}$, the compound underwent a degradation process, likely irreversible, that was still incomplete at $350\text{ }^\circ\text{C}$. Indeed, at $275\text{ }^\circ\text{C}$, peaks of CO_2 and NO_2 are clearly observable in the mass spectra (Figure 5). In contrast, no water loss was detected during this second process. Hence, the dehydration process was expected to be complete at $215\text{ }^\circ\text{C}$.

Reasonably, $150\text{ }^\circ\text{C}$ was selected as the operating dehydration temperature. Upon dehydration of CaHS in a furnace at $150\text{ }^\circ\text{C}$ under static air for 2 h, the FTIR spectrum of the dehydrated salt (CaHS-D) remained almost unchanged, except for the stretching vibration of (O–H) group-coordinated water molecules, which disappeared, as shown in Figure 6, proving that no material decomposition occurred at this selected temperature.

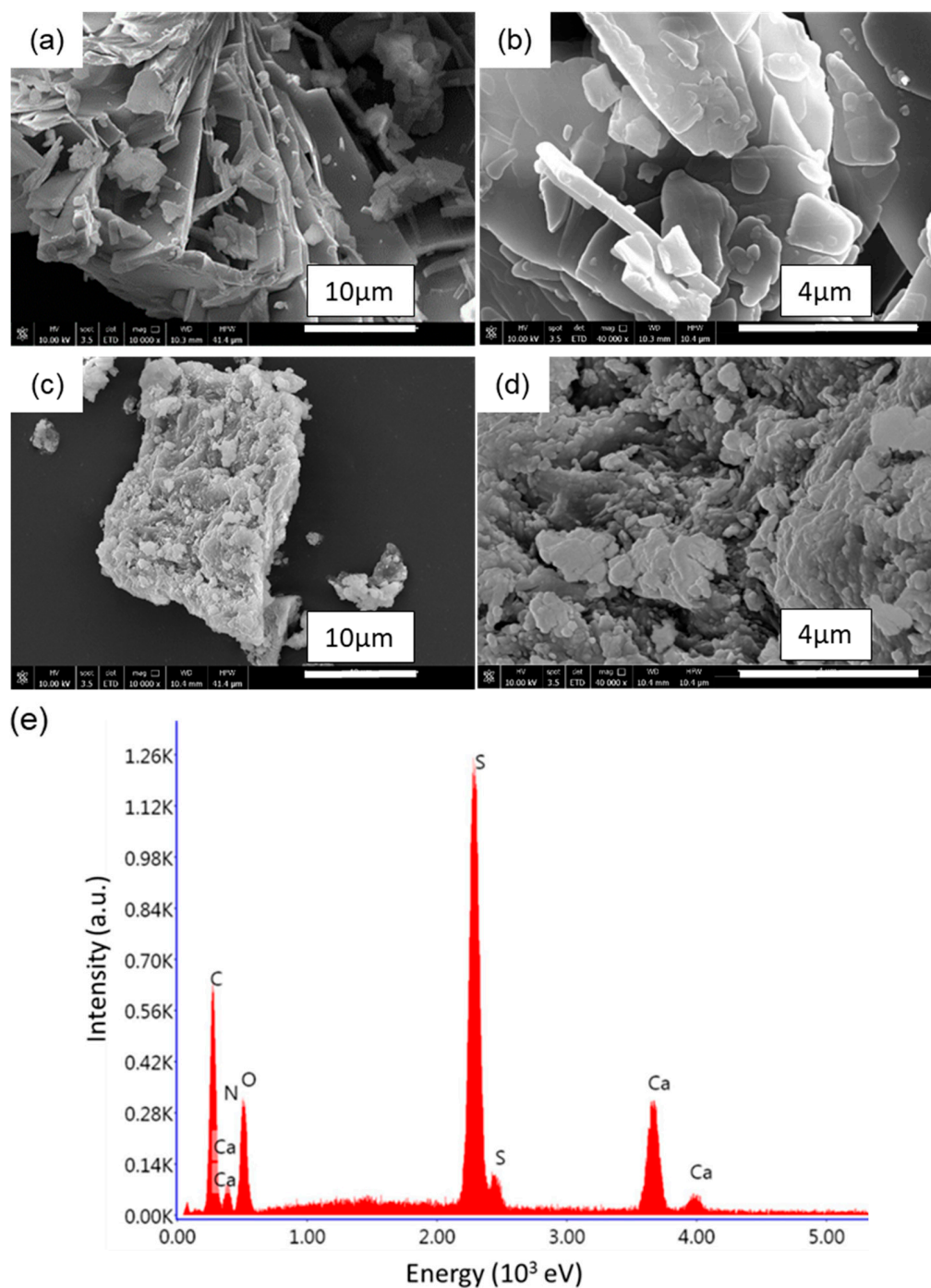


Figure 2. SEM micrographs of (a,b) Na₂HS and (c,d) CaHS with (e) EDX spectrum.

XRD analysis after the thermal treatment at 150 °C under static air for 2 h was indicative of an amorphous structure (see Figure S3 of ESI).

Furthermore, it is noteworthy that the CaHS did not suffer from deliquescence phenomena, even at an RH of ~100%. This was verified by introducing previously dehydrated (at 150 °C for 2 h, shown in Figure 7a) CaHS into a hydration chamber that consisted of a sample holder inside a sealed Teflon autoclave containing water for 2 h, in order to establish a gas–liquid equilibrium at 30 °C and a relative humidity (RH) of 100%. As shown in Figure 7b, the CaHS appears almost dry, and, macroscopically, powder granules/aggregates are distinguishable.

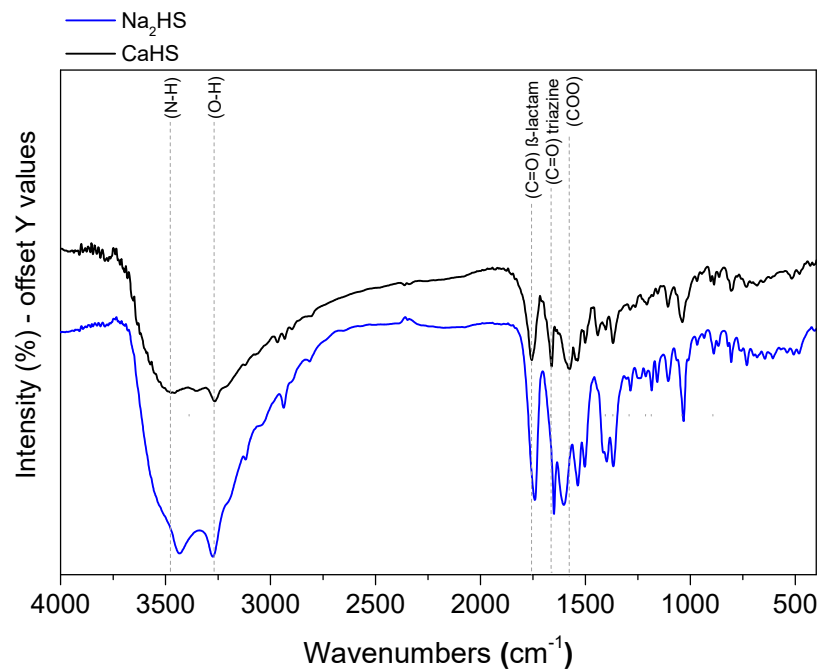


Figure 3. FTIR spectra of Na₂HS and CaHS.

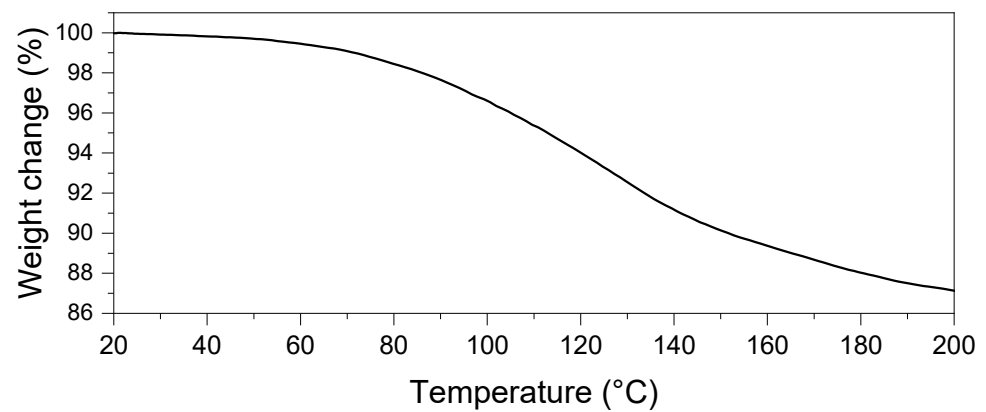


Figure 4. TG profile of CaHS under inert atmosphere (120 mL/min N₂) while heating the CaHS from r.T. to 200 °C.

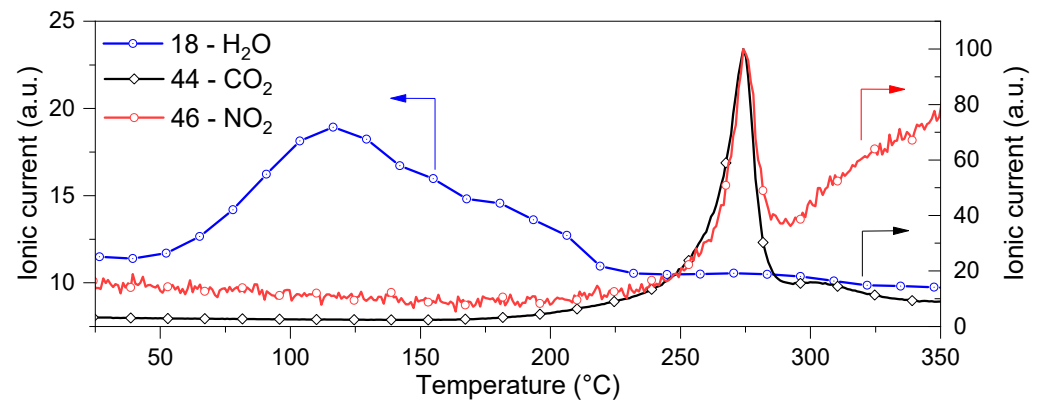


Figure 5. H₂O, CO₂, and NO_x mass spectra evolution profiles as functions of temperature while heating (10 °C/min) CaHS under an inert atmosphere (Ar 100 mL/min).

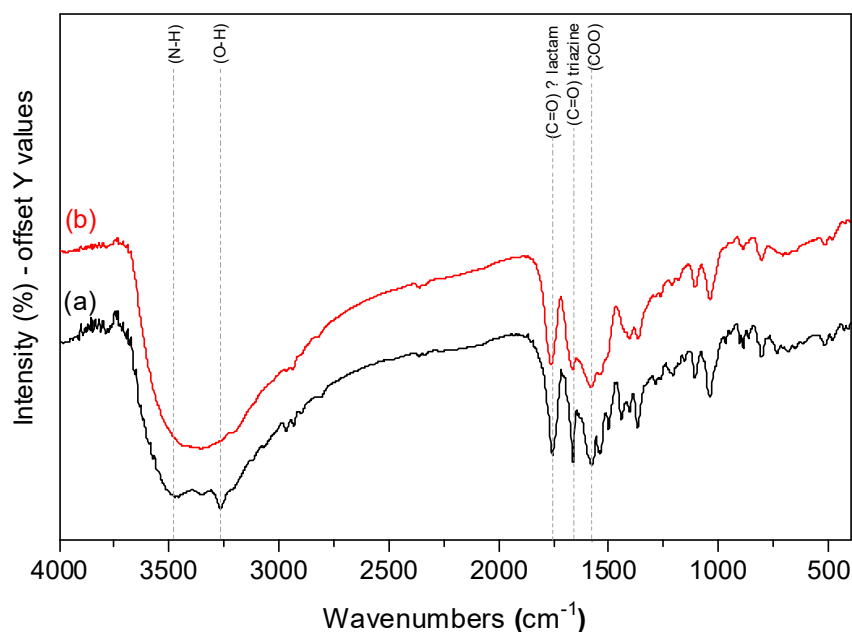


Figure 6. FTIR spectra of fresh (a) CaHS (black) and (b) CaHS-D obtained after thermal treatment at 150 °C for 2 h (red).

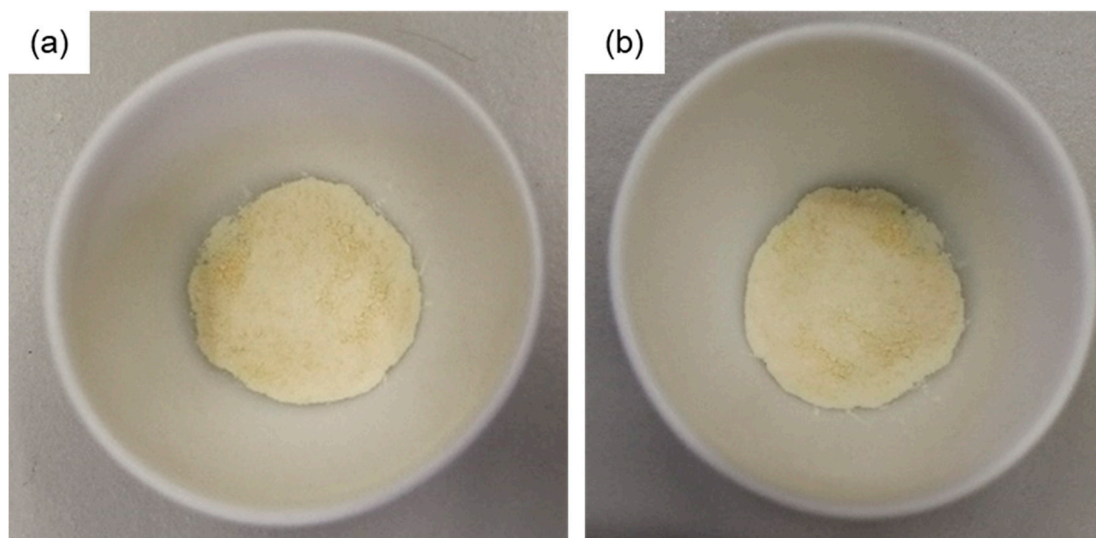


Figure 7. Pictures of CaHS (a) after the dehydration process in a furnace at 150 °C for 2 h and (b) after the rehydration process at 30 °C (RH = 100%) for 2 h.

3.3. Dehydration–Hydration Cycles

Dehydration–hydration cycles were carried out via a thermogravimetric dynamic vapor system under isothermal and isobaric conditions. For the isothermal experiment, a temperature of 30 °C was selected and the chamber RH was varied within the range of 0–90%. The results of three-cycle experiments are reported in Figure 8.

At 90% RH, the material was found to have a mass gain of ~20.45%, which corresponded to ~6.7 water molecules. This result is in agreement with the literature, where, accordingly, the maximum hydration number of this material is seven [22]. From the TG results (Figure 4), the as-synthesized material was found to have (a hydration number of 4.3, which is in agreement with the DVS results. Indeed, at an RH close to the one at which the material was synthesized (50%), the mass gain due to hydration was ~13.45%,

corresponding to ~ 4.4 water molecules, which was very close to the value obtained by the TG experiment ($\sim 13.1\%$, ~ 4.3 water molecules).

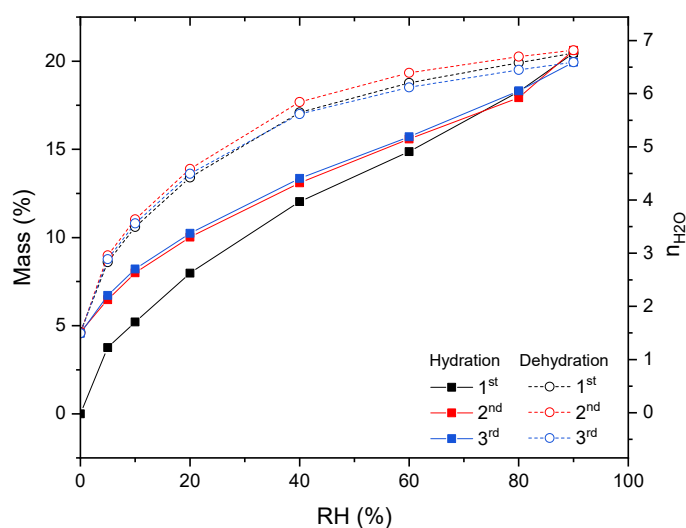


Figure 8. Hydration–dehydration cycles of CaHS through a thermogravimetric dynamic vapor system under isothermal conditions ($T = 30\text{ }^{\circ}\text{C}$) and varying the RH. Before the first hydration, the material was dehydrated at $150\text{ }^{\circ}\text{C}$ under a vacuum for 2 h.

After dehydration, namely reducing the RH to 0, a residual mass was observable that corresponds to ~ 1.5 water molecules. For achieving complete dehydration in an operationally relevant time range, a higher temperature than $30\text{ }^{\circ}\text{C}$ was required. Hence, under an isothermal dehydration–hydration cycle, the material could store/release about five water molecules. Further dehydration–hydration studies are ongoing at different temperatures and under isobaric conditions.

After the first cycle, the second and the third cycles profiles are comparable, thus indicating that material stability was achieved.

Hysteresis is observable between the dehydration and hydration reactions for the entire RH range, indicating a kinetic barrier. Generally, the presence of hysteresis between the sorption and desorption isotherms indicates that the water diffusion through the material structure is slower when the lattice re-arranges upon hydration [25]. This is applicable to CaHS; indeed, the material transforms from a completely amorphous structure to a more ordered one (see Figures 1 and S3) when it converts from the dehydrated to the hydrated form. Furthermore, due to this hysteresis, at equal temperatures, the difference in the relative humidity conditions under which the heat storage occurs and those at which the release phase takes place was extreme. This can prevent the material from dispersing the accumulated heat in the case of required intermediate operating conditions.

3.4. Heat Storage Capacity Evaluation

For a more comprehensive study, DSC analysis was carried out by heating the CaHS from $10\text{ }^{\circ}\text{C}$ up to $200\text{ }^{\circ}\text{C}$ by $10\text{ }^{\circ}\text{C}/\text{min}$. The thermogram, reported in Figure 9a, exhibited a broad endothermic peak which extended throughout the temperature range, and, from its deconvolution, four thermal events could be identified.

In order to determine the reaction enthalpy associated with the dehydration process of CaHS, and thus its heat storage capacity, DSC analysis was carried out under isothermal conditions at $150\text{ }^{\circ}\text{C}$. The setpoint temperature was rapidly achieved by heating at $30\text{ }^{\circ}\text{C}/\text{min}$ from $\sim 10\text{ }^{\circ}\text{C}$. A narrow endothermic peak was observed (Figure 9b), and the thermal event could be concluded after 20 min from the beginning of the experiment. Starting the analysis at a lower temperature allowed the measurement of the heat involved due to the water loss at r.T., which could not be evaluated by TG/DSC measurement. The estimated enthalpy of dehydration reaction of CaHS from heptahydrate to anhydrous

was $\sim 595.2 \text{ kJ/kg}_{\text{CaHS}}$ (or $\sim 427.8 \text{ kJ/mol}_{\text{CaHS}}$). Considering the measured value of bulk density of $1.6852 (\pm 0.002) \text{ g/cm}^3$, the volumetric heat storage capacity was estimated to be $\sim 278.6 \text{ kWh/m}^3$.

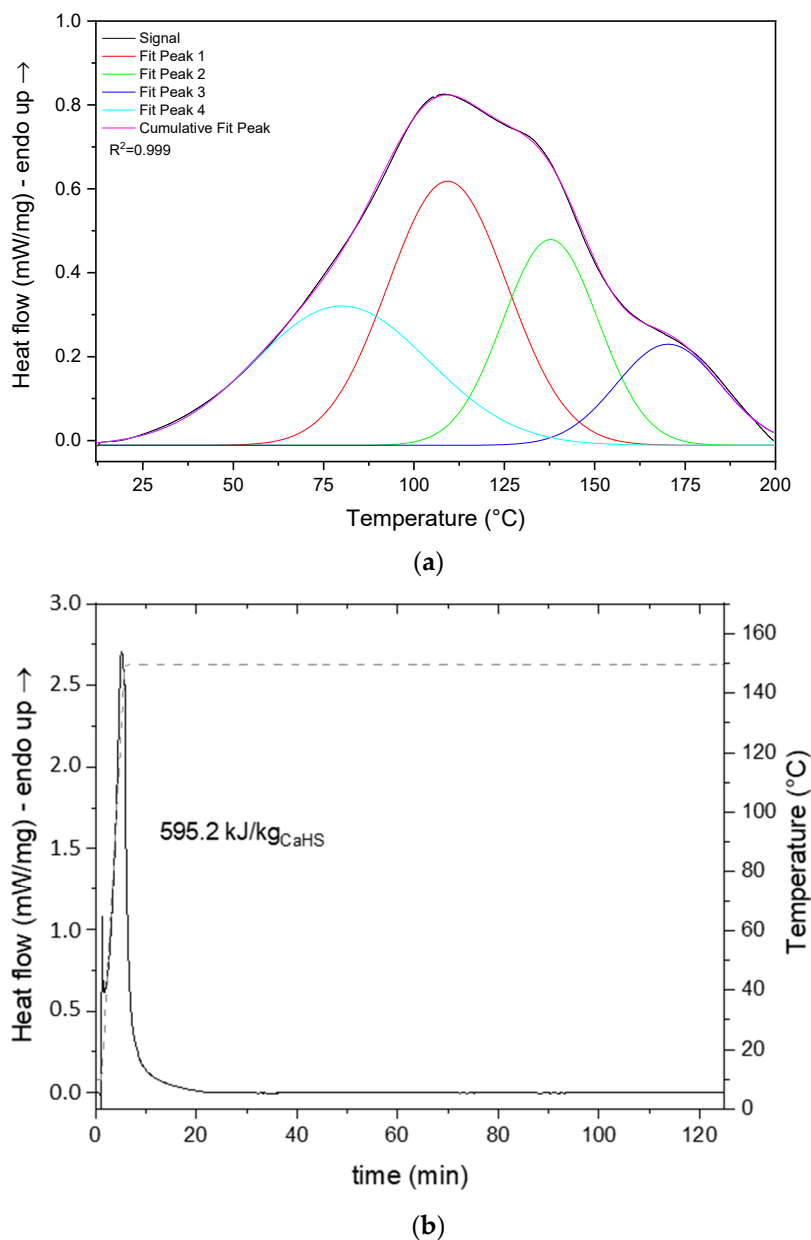


Figure 9. DSC thermogram of CaHS (a) under ramping and (b) isothermal conditions.

A comparison between CaHS and other selected common inorganic salt hydrates studied for thermochemical energy storage is reported in Table 1.

Compared to the most investigated inorganic salt hydrates listed here, CaHS offers a comparable level of heat storage (per mass and volume units) in line with the requirements for TES application and overcoming the deliquescence issue. Additionally, CaHS did not incur the risk of forming by-products in other salt hydrates that may suffer instability issues, such as Cl- and S-based salt hydrates. Indeed, chlorides, especially if dehydrated above $140 \text{ }^\circ\text{C}$, decompose and form volatile HCl, which may induce corrosion problems in the system [9,10]. Na_2S , despite its good storage capacity, evolves H_2S , which is toxic and corrosive [9,10]. Moreover, in CaHS, the Ca^{2+} ion is not susceptible to redox processes that can compromise efficiency, such as in CrCl_2 and FeCl_2 , where Cr^{2+} and Fe^{2+} ions tend to be oxidized in a humid environment [26,27].

Table 1. List of thermophysical characteristics (moles of H₂O involved in the dehydration process (n); molar enthalpy of dehydration per moles of material (ΔH (kJ/mol)); heat storage capacity per mass (Q^M); and volume (Q^V) of material) and working conditions (dehydration (T_{deh}) and hydration (T_{hyd}) temperatures) of CaHS and other selected common inorganic salt hydrates.

Compound	n	ΔH (kJ/mol)	Q^M (kJ/kg)	Q^V (kWh/m ³)	T_{deh} (°C)	T_{hyd} (°C)	Ref.
CaHS · 7H ₂ O	4.3	427.8	595.2	278.6	150	30	this study
SrBr ₂ · 6H ₂ O	5	337.0	947.9	433.5	52	45	[3–5]
SrCl ₂ · 2H ₂ O	1	59.0	302.4	164.1	52	46	[3–5]
MgSO ₄ · 6H ₂ O	4	225.1	986.4	558.0	91–123	10	[3–5]
MgCl ₂ · 6H ₂ O	1.3	71.5	351.7	153.3	104	61	[4,8]
CaCl ₂ · 2H ₂ O	2	125.0	837.0	542.5	111	63	[4,8]
LiCl · H ₂ O	1	62.9	1041.2	486.0	80	73	[4]
K ₂ CO ₃ · 1.5H ₂ O	1.5	95.5	579.6	355.6	65	59	[4]
Na ₂ S · 5H ₂ O	3	188.7	1120.3	780.6	73	66	[3,4]

Furthermore, CaHS operating conditions are less limiting with respect to other inorganic salts. Indeed, the deliquescence phenomena are not observable even at high RH values, and no decomposition is detectable below 150 °C. Additionally, a critical dehydration temperature may limit the efficiency of an inorganic system—for example, the equilibrium of the MgSO₄–H₂O couple is, indeed, very close to the pressure–temperature equilibrium curve of water; hence, in real operating systems, the small difference between the applied temperature for the hydration process and the resulting discharged one compromises the efficiency of systems based on this salt [10]. Comprehensibly, concerns may arise due to the cost of this specific salt, which was synthesized from commercial disodium triaxone. Nevertheless, in light of the reported results, this study opens new paths for the exploration of, organic salt hydrates, a new class of materials, for TES application. CaHS, which was selected as a model molecule, exhibits interesting heat storage capacity, thermal stability in a broad temperature range, and safety from common problems typical of inorganic salt hydrates (such as deliquescence).

4. Conclusions

We propose for the first time the use of an organic hydrated salt as a candidate material for thermochemical energy storage, specifically calcium;7-[[2-(2-amino-1,3-thiazol-4-yl)-2-methoxyiminoacetyl]amino]-3-[(2-methyl-5,6-dioxo-1H-1,2,4-triazin-3-yl)sulfanylmethyl]-8-oxo-5-thia-1-azabicyclo[4.2.0]oct-2-ene-2-carboxylate, known as calcium ceftriaxone, which we named CaHS (calcium hydrated salt) and used as our model compound. This material undergoes reversible dehydration–hydration reactions. The operating dehydration temperature range, 30–150 °C, similar to that of inorganic salt hydrates, is suitable for low-/middle-temperature thermochemical energy storage applications. In such a context, systems that waste (e.g., industrial processes) or produce (e.g., solar thermal panels) heat within this temperature range could be the potential users of this TCM. In comparison to its inorganic counterparts, CaHS is stable upon exposure at an RH of 100% at 30 °C, assuring no drawbacks related to deliquescence phenomena and, at the same time, fully recovering its hydration uptake at low temperature. Additionally, CaHS does not show any decomposition under the operating conditions, avoiding the need for any preventive strategy (e.g., limitation of maximum charging temperature, working at a low heating rate for the discharging step, using porous matrices, etc.). The material heat storage capacity (~595.2 kJ/kg_{CaHS}) is comparable with that of other inorganic salt hydrates, without appreciable efficiency losses in terms of energy as cycles are performed due to unconverted material.

Such encouraging results strongly support the idea of considering hydrated organic salts for effective TCS applications, breaking new ground for this field of research. Further studies are ongoing for better understanding the material’s behavior at different

dehydration–hydration temperatures and under isobaric conditions, as well as its stability upon several hydration–dehydration cycles.

Supplementary Materials: The following supporting information can be downloaded at: <https://www.mdpi.com/article/10.3390/en15124339/s1>. Figure S1: XRD diffractogram of CaHS after thermal treatment at 1000 °C. Figure S2: DVS RH(%) profiles as function of time. Figure S3: XRD diffractogram of dehydrated CaHS. Table S1: List of the d-spacing and Miller indexes for Na₂HS (JCPDS # 71-1637). Table S2: List of calculated d-spacing for CaHS.

Author Contributions: Conceptualization, C.M. and E.P. (Edoardo Proverbio); methodology, E.M. and E.P. (Elpida Piperopoulos); validation, E.M., E.L.M., D.P., D.I. and E.P. (Elpida Piperopoulos); formal analysis, E.M., D.P. and E.P. (Elpida Piperopoulos); investigation, E.M., D.P. and E.P. (Elpida Piperopoulos); resources, C.M. and E.P. (Edoardo Proverbio); data curation, E.M., D.P. and E.P. (Elpida Piperopoulos); writing—original draft preparation, E.M., E.P. (Elpida Piperopoulos) and C.M.; writing—review and editing, E.M., E.P. (Elpida Piperopoulos), and C.M.; supervision, E.P. (Edoardo Proverbio) and C.M.; project administration, C.M.; funding acquisition, C.M. All authors have read and agreed to the published version of the manuscript.

Funding: This research was funded by INSTM (Consorzio Interuniversitario Nazionale per la Scienza e Tecnologia dei Materiali), within the project “Thermochemical materials for heat storage: development and characterization”, grant number INSTMME002 and by PON “Ricerca e Innovazione 2014 e 2020”, Project ARS01_00334 NAUSICA—NAvi efficienti tramite l’Utilizzo di Soluzioni tecnologiche Innovative e low Carbon, CUP B45F21000700005.

Institutional Review Board Statement: Not applicable.

Informed Consent Statement: Not applicable.

Data Availability Statement: All data generated or analyzed during this study are included in this published article.

Acknowledgments: This study was conducted as part of the project “Thermochemical materials for heat storage: development and characterization” sponsored by INSTM (Consorzio Interuniversitario Nazionale per la Scienza e Tecnologia dei Materiali), within the IEA SHC Task 67 “Compact Thermal Energy Storage Materials” and PON “Ricerca e Innovazione 2014 e 2020”, Project ARS01_00334 NAUSICA—NAvi efficienti tramite l’Utilizzo di Soluzioni tecnologiche Innovative e low Carbon.

Conflicts of Interest: The authors declare no conflict of interest.

References

1. Piperopoulos, E.; Mastronardo, E.; Fazio, M.; Lanza, M.; Galvagno, S.; Milone, C. Synthetic strategies for the enhancement of Mg(OH)₂ thermochemical performances as heat storage material. *Energy Procedia* **2018**, *155*, 269–279. [[CrossRef](#)]
2. Lahmidi, H.; Mauran, S.; Goetz, V. Definition, test and simulation of a thermochemical storage process adapted to solar thermal systems. *Sol. Energy* **2006**, *80*, 883–893. [[CrossRef](#)]
3. N’Tsoukpoe, K.E.; Liu, H.; Le Pierrès, N.; Luo, L. A review on long-term sorption solar energy storage. *Renew. Sustain. Energy Rev.* **2009**, *13*, 2385–2396. [[CrossRef](#)]
4. Letcher, T.M. Storing Energy, with Special Reference to Renewable Energy Sources. *Chem. Int.* **2016**, *38*, 28. [[CrossRef](#)]
5. Pinel, P.; Cruickshank, C.A.; Beausoleil-Morrison, I.; Wills, A. A review of available methods for seasonal storage of solar thermal energy in residential applications. *Renew. Sustain. Energy Rev.* **2011**, *15*, 3341–3359. [[CrossRef](#)]
6. Wang, X.; Li, B.; Qu, Z.; Zhang, J.; Jin, Z. Effects of graphite microstructure evolution on the anisotropic thermal conductivity of expanded graphite/paraffin phase change materials and their thermal energy storage performance. *Int. J. Heat Mass Transf.* **2020**, *155*, 119853. [[CrossRef](#)]
7. Farulla, G.A.; Cellura, M.; Guarino, F.; Ferraro, M. A Review of Thermochemical Energy Storage Systems for Power Grid Support. *Appl. Sci.* **2020**, *10*, 3142. [[CrossRef](#)]
8. Tescari, S.; Lantin, G.; Lange, M.; Breuer, S.; Agrafiotis, C.; Roeb, M.; Sattler, C. Numerical Model to Design a Thermochemical Storage System for Solar Power Plant. *Energy Procedia* **2015**, *75*, 2137–2143. [[CrossRef](#)]
9. Tatsidjodoung, P.; Le Pierrès, N.; Luo, L. A review of potential materials for thermal energy storage in building applications. *Renew. Sustain. Energy Rev.* **2013**, *18*, 327–349. [[CrossRef](#)]
10. N’Tsoukpoe, K.E.; Schmidt, T.; Rammelberg, H.U.; Watts, B.A.; Ruck, W.K. A systematic multi-step screening of numerous salt hydrates for low temperature thermochemical energy storage. *Appl. Energy* **2014**, *124*, 1–16. [[CrossRef](#)]
11. Mehrabadi, A.; Farid, M. New salt hydrate composite for low-grade thermal energy storage. *Energy* **2018**, *164*, 194–203. [[CrossRef](#)]

12. Lele, A.F. *A Thermochemical Heat Storage System for Households*; Springer: Cham, Switzerland, 2016. [[CrossRef](#)]
13. Kohler, T.; Biedermann, T.; Müller, K. Experimental Study of $\text{MgCl}_2 \cdot 6 \text{H}_2\text{O}$ as Thermochemical Energy Storage Material. *Energy Technol.* **2018**, *6*, 1935–1940. [[CrossRef](#)]
14. Frazzica, A.; Cabeza, L.F. *Recent Advancements in Materials and Systems for Thermal Energy Storage—An Introduction to Experimental Characterization Methods*; Springer International Publishing: New York, NY, USA, 2019. [[CrossRef](#)]
15. Mastronardo, E.; Bonaccorsi, L.; Kato, Y.; Piperopoulos, E.; Lanza, M.; Milone, C. Strategies for the enhancement of heat storage materials performances for $\text{MgO}/\text{H}_2\text{O}/\text{Mg}(\text{OH})_2$ thermochemical storage system. *Appl. Therm. Eng.* **2017**, *120*, 626–634. [[CrossRef](#)]
16. Druske, M.-M.; Fopah-Lele, A.; Korhammer, K.; Rammelberg, H.U.; Wegscheider, N.; Ruck, W.; Schmidt, T. Developed Materials for Thermal Energy Storage: Synthesis and Characterization. *Energy Procedia* **2014**, *61*, 96–99. [[CrossRef](#)]
17. Zbair, M.; Bennici, S. Survey Summary on Salts Hydrates and Composites Used in Thermochemical Sorption Heat Storage: A Review. *Energies* **2021**, *14*, 3105. [[CrossRef](#)]
18. Casey, S.P.; Elvins, J.; Riffat, S.; Robinson, A. Salt impregnated desiccant matrices for ‘open’ thermochemical energy storage—Selection, synthesis and characterisation of candidate materials. *Energy Build.* **2014**, *84*, 412–425. [[CrossRef](#)]
19. Michel, B.; Neveu, P.; Mazet, N. Comparison of closed and open thermochemical processes, for long-term thermal energy storage applications. *Energy* **2014**, *72*, 702–716. [[CrossRef](#)]
20. Gaeini, M.; Rouws, A.; Salari, J.; Zondag, H.; Rindt, C. Characterization of microencapsulated and impregnated porous host materials based on calcium chloride for thermochemical energy storage. *Appl. Energy* **2018**, *212*, 1165–1177. [[CrossRef](#)]
21. Owens, H.M.; Dash, A.K. Ceftriaxone Sodium: Comprehensive Profile. *Profiles Drug Subst. Excipients Relat. Methodol.* **2003**, *30*, 21–57. [[CrossRef](#)]
22. Refat, M.S.; Altalhi, T.; Fetooh, H.; Alsuhaibani, A.M.; Hassan, R.F. In neutralized medium five new Ca(II), Zn(II), Fe(III), Au(III) and Pd(II) complexity of ceftriaxone antibiotic drug: Synthesis, spectroscopic, morphological and anticancer studies. *J. Mol. Liq.* **2020**, *322*, 114816. [[CrossRef](#)]
23. Katz, K.A.; Glusker, J.P.; Beebe, S.A.; Bock, C.W. Calcium Ion Coordination: A Comparison with That of Beryllium, Magnesium, and Zinc. *J. Am. Chem. Soc.* **1996**, *118*, 5752–5763. [[CrossRef](#)]
24. Gonzalez, D.; Golab, J.T.; Eilert, J.Y.; Wang, R.; Kaduk, J.A. Crystal structure of ceftriaxone sodium hemiheptahydrate, $\text{C}_{18}\text{H}_{16}\text{N}_8\text{O}_7\text{S}_3\text{Na}_2(\text{H}_2\text{O})_{3.5}$. *Powder Diffr.* **2020**, *35*, 206–212. [[CrossRef](#)]
25. Tieger, E.; Kiss, V.; Pokol, G.; Finta, Z.; Dušek, M.; Rohlíček, J.; Skořepová, E.; Brázda, P. Studies on the crystal structure and arrangement of water in sitagliptin-tartrate hydrates. *CrystEngComm* **2016**, *18*, 3819–3831. [[CrossRef](#)]
26. Clark, R.-J.; Mehrabadi, A.; Farid, M. State of the art on salt hydrate thermochemical energy storage systems for use in building applications. *J. Energy Storage* **2019**, *27*, 101145. [[CrossRef](#)]
27. Donkers, P.; Sögütöglu, L.; Huinink, H.; Fischer, H.; Adan, O. A review of salt hydrates for seasonal heat storage in domestic applications. *Appl. Energy* **2017**, *199*, 45–68. [[CrossRef](#)]